Ophiopogonin B induces gastric cancer cell death by blocking the GPX4/xCT-dependent ferroptosis pathway

LIYI ZHANG[1], CHUNLEI LI[1], YUZHAN ZHANG[2], JINWEN ZHANG[3] and XIAOLEI YANG[4]

[1]Department of Internal Medicine, Jiaozhou Central Hospital, Qingdao, Shandong 266300; [2]Department of Cardiothoracic Surgery, Shanxian Dongda Hospital, Heze, Shandong 274300; [3]Department of Laboratory Medicine, Heze Hospital of Traditional Chinese Medicine, Heze, Shandong 274000; [4]Department of General Surgery, 80th Army Hospital, Weifang, Shandong 261021, P.R. China

Received September 3, 2021; Accepted December 8, 2021

DOI: 10.3892/ol.2022.13224

Abstract. Ophiopogonin B (OP-B) is extensively applied as a treatment for pulmonary disease and is reported to suppress lung cancer. However, further study is needed to determine whether OP-B suppresses gastric cancer (GC). The mRNA levels of prostaglandin-endoperoxide synthase 2 (Ptgs2) and ChaC glutathione-specific gamma-glutamylcyclotransferase 1 (Chac1) were determined using quantitative PCR. Ptgs2 and Chac1 mRNA levels were significantly increased in GC cancer tissues compared with those of adjacent normal controls. The CCK-8 assay revealed that OP-B suppressed GC cell viability in a time- and dose-dependent manner. The administration of OP-B in combination with different cell death inhibitors showed that only the ferroptosis inhibitor, ferrostatin-1 (Fer-1), abolished the OP-B-induced death of both AGS and NCI-N87 cells, but not other inhibitors. Western blot analysis indicated that OP-B reduced the expression of glutathione peroxidase 4 (GPX4) and solute carrier family 7 member 11 (SLC7A11, xCT) but had no effects on the expression of nuclear receptor coactivator 4 (NCOA4) and ferritin heavy chain 1 (FTH1) in AGS and NCI-N87 cells. *In vivo* administration of OP-B reduced the volume and weight of AGS tumors. In addition, the expression of GPX4 and xCT was reduced in nude mice treated with OP-B compared with control mice. In summary, results of the present study suggest that OP-B induces ferroptosis in gastric cancer cells by blocking the GPX4/xCT system.

Introduction

Gastric cancer (GC) is the second most common cancer in China and ranks as the fourth most common type of malignant cancer worldwide (1,2). Although the survival rate is improved when patients are treated with radiotherapy, chemotherapy and targeted therapy after surgery, the overall survival rate of patients with advanced GC remains low (3). Thus, an understanding of the molecular mechanisms and identification of potential therapeutic targets is very important for GC therapy.

Ferroptosis is a newly identified form of programmed cell death that is mediated by excess iron-dependent lipid peroxidation (4,5). Glutathione peroxidase 4 (GPX4), a glutathione (GSH)-dependent selenoenzyme, prevents ferroptosis by changing toxic lipid hydroperoxides into nontoxic lipid alcohols (6,7). Once GPX4 activity is suppressed, the products of lipid peroxidation increase significantly, subsequently resulting in ferroptosis (8,9). Solute carrier family 7 member 11 (SLC7A11, xCT) is a sodium-independent cystine-glutamate antiporter that transfers extracellular cystine into cells, which is then processed into cysteine, a rate-limiting substrate for glutathione (GSH) synthesis (10,11). Nuclear receptor coactivator 4 (NCOA4) is a component of autophagosomes and is reported to mediate ferritinophagy by interacting with surface arginine residues in ferritin heavy chain 1 (FTH1) (12,13). NCOA4 overexpression induces ferroptosis by increasing intracellular-free iron contents, glutathione production and reactive oxygen species (ROS) levels (14). Ferroptosis plays a key role in various diseases, including GC (15-17). Targeting ferroptosis may be a potential therapeutic strategy for patients with GC.

Ophiopogonin B (OP-B) is extracted from Radix *Ophiopogon japonicus*, which has been extensively applied as a treatment for pulmonary disease in the past in Southeast Asia. OP-B has been reported to exert anticancer effects on different cancer types (18,19). For instance, in colon cancer, OP-B suppresses cancer cell proliferation and migration by activating JNK/c-Jun signaling (18). In lung cancer cells, OP-B exerts anticancer effects by inducing apoptosis, mitotic catastrophe and autophagy (19). Previous findings showed that OP-B suppresses the proliferation of SGC-7901 human GC cells (20). However, SGC-7901 cells are reported to be contaminated with HeLa cells. Thus, we explored whether OP-B suppresses GC cells and the potential underlying mechanism.

Correspondence to: Dr Xiaolei Yang, Department of General Surgery, 80th Army Hospital, 256 Beigong West Street, Weifang, Shandong 261021, P.R. China
E-mail: weiaixiaohua123@163.com

Key words: ophiopogonin B, gastric cancer, glutathione peroxidase 4, ferroptosis

Materials and methods

Patient samples. A total of 60 GC and adjacent normal control tissues (>5 cm away from the edge of cancer tissues and pathologically confirmed as normal gastric mucosa) were selected. Once the specimens were removed, they were immediately stored in RNAsaver (Beijing Solarbio Science and Technology Co., Ltd.) at -80˚C to minimize RNA degradation. The 60 patients with GC were aged 42-85 years with an average age of 58.9±23.7 years, and included 32 males and 28 females. The inclusion criteria were: i) Age ≥18 years; ii) absence of radiotherapy, chemotherapy or any adjuvant therapy before hospitalization; iii) absence of other malignant tumors; and iv) absence of a family history of genetic diseases. Exclusion criteria were: i) Antibiotics <3 months before blood collection; ii) liver insufficiency and iii) autoimmune system deficiency. In terms of the degree of tissue differentiation, 32 cases of high and moderate differentiation and 28 cases of low and no differentiation were identified.

In terms of the tumor-node-metastasis (TNM) stage, 25 cases were in stage I-II and 35 cases were in stage III-IV. None of the patients underwent chemotherapy, radiotherapy or immunotherapy prior to surgery, and all of the patients were diagnosed via routine histopathology after the operation. The clinicopathological types of GC patients were summarized as follows: 2 cases of papillary adenocarcinoma, 25 cases of well-differentiated adenocarcinoma, 5 cases of moderately differentiated adenocarcinoma, 24 cases of poorly differentiated adenocarcinoma, 2 cases of signet-ring cell carcinoma, 2 cases of mucinous carcinoma.

All 60 patients signed the informed consent form, and the study was approved by the Ethics Committee of Jiaozhou Central Hospital (approval no. JZCH-2019JHU4).

Cell culture. The human gastric cancer cell lines AGS and NCI-N87 were purchased from the American Type Culture Collection (ATCC). The normal human gastric epithelium cell line (GES-1) was purchased from Procell Life Science & Technology Co., Ltd. (CL-0563). Cell authenticity was identified using STR files. Cells were cultured at 37˚C with Dulbecco's modified Eagle's medium (DMEM) (HyClone; GE Healthcare Life Sciences) supplemented with 10% fetal bovine serum (HyClone; GE Healthcare Life Sciences), 100 U/ml penicillin (HyClone; GE Healthcare Life Sciences) and 100 g/ml streptomycin (HyClone; GE Healthcare Life Sciences) in a humidified atmosphere containing 5% CO_2.

Cell Counting Kit-8 (CCK-8) assay. AGS and NCI-N87 cells were seeded in a 96-well plate at a density of 3,000 cells/well. After incubation for 24 h at 37˚C, the cells were treated with OP-B (MW: 722.9, HPLC ≥98%, abs47001825, Absin Biotech. Co.) at the indicated concentrations (0.00, 0.25, 0.50, 1.00, 2.00, 4.00, 8.00, 16.00, 32.00 and 64.00 μM for AGS; 0, 1, 2, 4, 8, 16, 32 and 64 μM NCI-N87).

In addition, AGS and NCI-N87 cells were preincubated with 10 μM zVAD, 10 μM 3-MA, 10 μM for Nec-1or 1 μM Fer-1 for 1 h. AGS and NCI-N87 cells were treated with 10 or 20 μM OP-B for 24 h, respectively. Subsequently, 10 μl of CCK-8 solution (C0038, Beyotime Biotech) was incubated with the cells for 2 h before harvest. A Bio-Tek microplate reader (Winooski) was used to read the optical density (OD) value at 490 nm. Half maximal inhibitory concentration (IC_{50}) was calculated as: Cell inhibition rate (%)=1-(experimental group OD value/normal group OD value)x100%.

Cell apoptosis analysis. After treatment with OP-B for 24 h, AGS and NCI-N87 cells were washed with 1X PBS three times and stained with an Annexin V-PE/7-AAD apoptosis kit (E-CK-A216, Elabsience) according to the manufacturer's protocol. The following controls were used to set up compensation and quadrants: i) Unstained cells; ii) Cells stained with PE Annexin V (no 7-AAD); iii) Cells stained with 7-AAD (no PE Annexin V). Cells were analyzed using an FC500 flow cytometer equipped with CXP software (Beckman Coulter). According to the instructions, Q1 represented 7-AAD+/PE-cells; Q2 represented PE+/7-ADD+ cells (necrosis and late apoptosis cells); Q3 represented PE+/7-ADD-cells (early apoptosis cells); Q4 represented PE-/7-AAD-cells (living cells). Death cells were calculated as: the necrosis and late apoptosis cells (Q2) + early apoptosis cells (Q3).

Western blot analysis. Total protein were collected from AGS and NCI-N87 cells in a radioimmunoprecipitation assay buffer (Beijing Solarbio Science and Technology Co., Ltd.). The protein concentration was determined using a BCA protein assay kit (Pierce; Thermo Fisher Scientific, Inc.). A total of 30 μg protein was separated on 10% SDS-PAGE gels, followed by transfer of electrophoresed proteins onto nitrocellulose membranes. The membranes were blocked with 5% non-fat milk (Beyotime Biotechnology, Beijing, China) and incubated with primary antibodies, including GPX4 (no. 52455, 1:1,000, Cell Signaling Technology, Inc.), xCT (no. 12691, 1:1,000, Cell Signaling Technology, Inc.), NCOA4 (no. 66849; 1:1,000; Abcam), FTH-1 (no. 4393; 1:1,000; Abcam), and GAPDH (cat. no. 5174, 1:4,000, Cell Signaling Technology, Inc.), at 4˚C overnight. Subsequently, the cells were incubated with the corresponding peroxidase-conjugated secondary antibodies (both 1:5,000; cat. no. ZB-2301 and ZB-2305; Beijing Zhongshan Golden Bridge Biotechnology Co.). The protein bands were detected using enhanced chemiluminescence reagent (EMD Millipore). Relative protein expression was normalized to GAPDH. All the experiments were repeated three times. ImageJ 1.43b software (National Institutes of Health) was used for the densitometry analysis.

Quantitative PCR. A total of $5x10^6$ cells were collected in EP tubes without RNase (Qiagen GmbH) and lysed with RNAVzol (Vigorous Biotechnology Beijing Co., Ltd.). Chloroform (Vigorous Biotechnology Beijing Co., Ltd.) was added for 15 sec, incubated at room temperature for 10 min, and centrifuged at 13,000 x g for 10 min at 4˚C. Then, the supernatant was absorbed, and an equal volume of isopropanol was added. The mixture was gently agitated and incubated at room temperature for 10 min. The cells were centrifuged at 13,000 x g for 10 min at 4˚C. The supernatant was then discarded carefully, and the sample precipitated by washing with 1 ml of 75% ethanol. Subsequently, the supernatant was discarded after centrifugation at 13,000 x g for 3 min at 4˚C, and the pellet was dissolved in 20 μl of DEPC H_2O. The RNA (1 μg) was reverse transcribed into cDNAs. The target

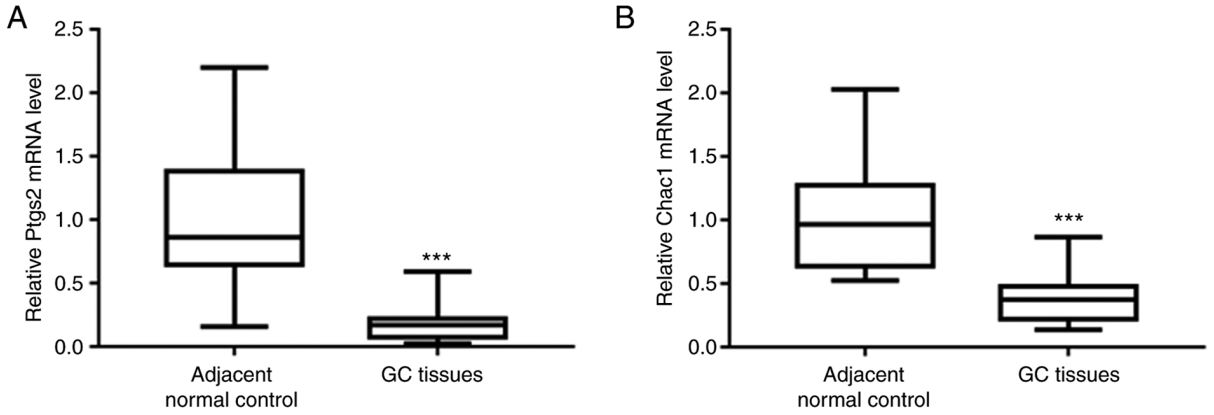

Figure 1. Ptgs2 and Chac1 mRNA levels were detected in GC tissues and adjacent normal control tissues. qPCR analysis revealed significantly reduced levels of (A) Ptgs2 and (B) Chac1 mRNAs in GC tissues compared with those in adjacent normal control tissues. ***P<0.001 compared with adjacent normal control tissues.

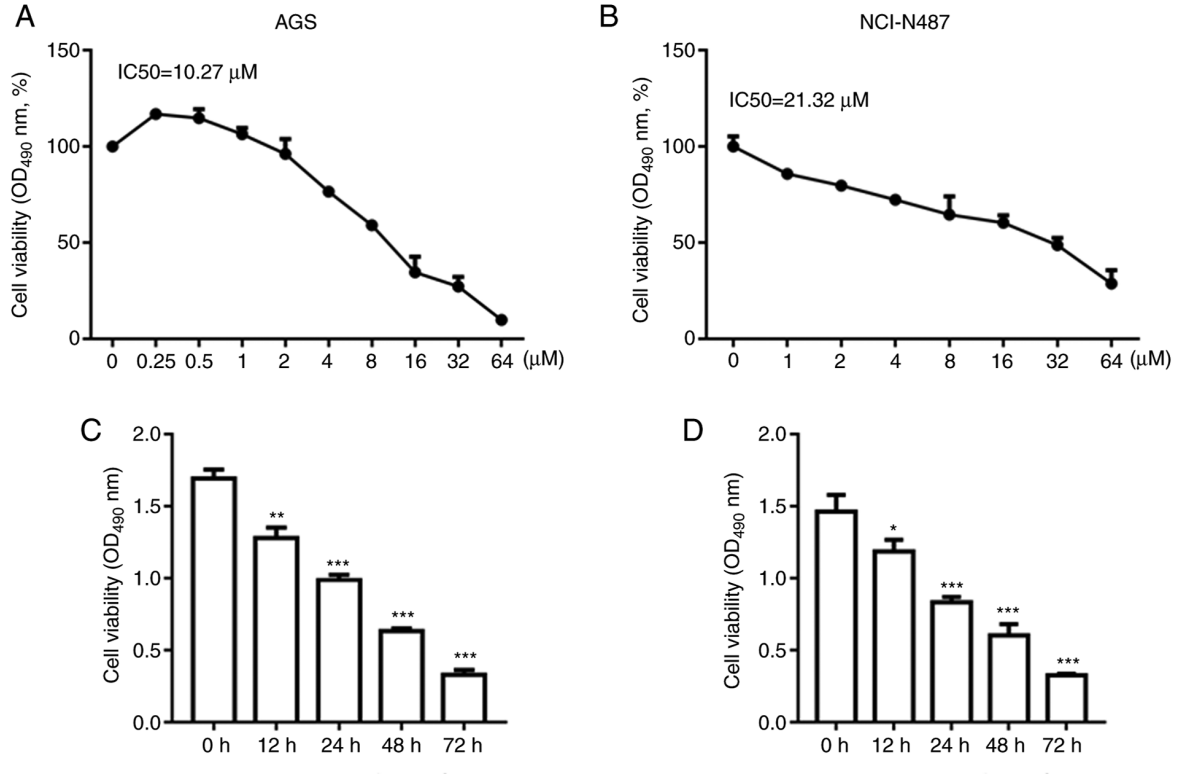

Figure 2. OP-B reduced AGS and NCI-N87 cell viability in a dose- and time-dependent manner. The CCK-8 assay indicated that OP-B decreased the viability of (A) AGS and (B) NCI-N87 cells in a dose-dependent manner. OP-B also decreased the viability of (C) AGS and (D) NCI-N87 cells in a time-dependent manner. *P<0.05, **P<0.01, and ***P<0.001 compared with 0 h.

fragment was amplified using PCR. The reaction system had a total volume of 20 μl, including 10 μl of 2X QuantiTect SYBR Green PCR Master Mix (Bio-Rad Laboratories, Inc.), 0.25 μl of 10 μM forward primer, 0.25 μl of reverse primer, 5 μl of cDNAs, and 4.75 μl of DEPC H_2O. The reaction conditions were: predenaturation at 95˚C for 15 min and 40 cycles of denaturation at 94˚C for 30 sec, annealing at 60˚C for 30 sec, and extension at 68˚C for 30 sec. Each experiment was repeated three times. The primers used in the study were as follows: GAPDH-F: 5'-ACCACAGTCCATGCCATCAC-3';-R: 5'-CTAGACGGCAGGTCAGGTC-3'; Ptgs2-F: 5'-GAGGGATCTGTGGATGCTTCG-3';-R: 5'-AAACCCACAGTGCTTGACAC-3'; Chac1-F: 5'-CCCCATCCTGGAACTTGACC-3';-R: 5'-CTATGGATGGCTGGGCTGAG-3'.

Quantification of MDA, ROS, and Fe^{2+} levels. Briefly, AGS and NCI-N87 cells were seeded in 6-well culture dishes at a density of $2x10^6$ cells/well and incubated overnight at 37˚C. The cells were preincubated with or without 1 μM ferrostatin-1 (Fer-1, HY-100579, MedChemExpress) for 1 h. Subsequently, 10 or 20 μM OP-B was added to AGS and NCI-N87 cells and incubated for another 24 h at 37˚C. Subsequently, the MDA [Lipid Peroxidation (MDA) Assay Kit, ab118970, Abcam], ROS [DCFDA/H_2DCFDA Cellular ROS Assay kit, ab113851, Abcam,

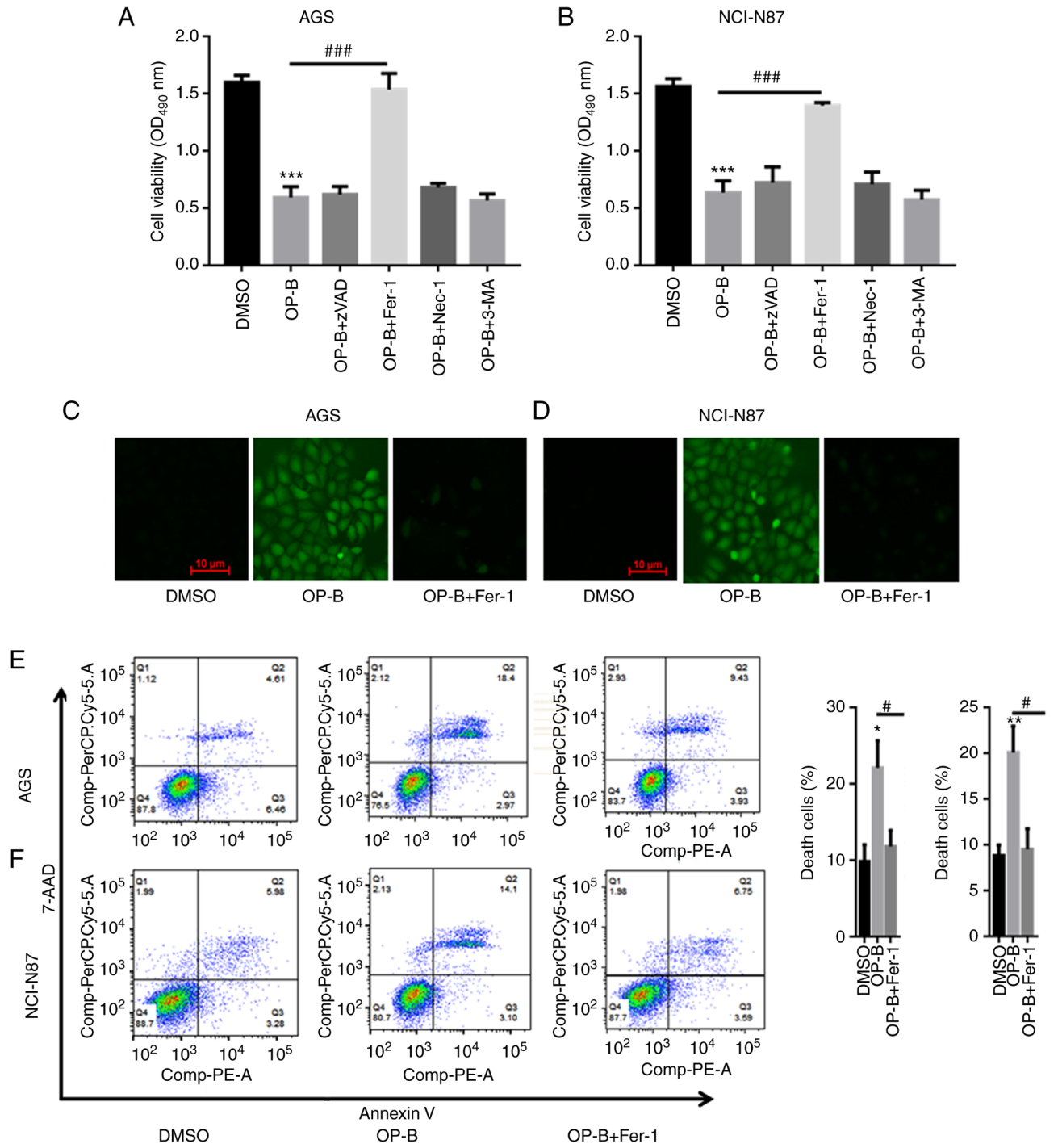

Figure 3. OP-B induced ferroptosis in AGS and NCI-N87 cells. Preincubation with Fer-1 reversed OP-B-induced (A) AGS and (B) NCI-N87 cell death. DCFDA staining showed that OP-B increased ROS production in (C) AGS and (D) NCI-N87 cells. OP-B significantly induced (E) AGS and (F) NCI-N87 cell death, but preincubation with Fer-1 partially reversed OP-B-induced GC cell death. *P<0.05, **P<0.01, and ***P<0.001 compared with DMSO; $^{\#}$P<0.05, $^{\#\#\#}$P<0.001 vs. OP-B group.

Cambridge, UK] and Fe^{2+} [Iron Assay Kit, ab83366, Abcam] contents were measured using kits according to the protocol.

ROS staining. Briefly, AGS and NCI-N87 cells were seeded in 6-well culture dishes at a density of $2x10^6$ cells/well and incubated overnight at 37˚C. The cells were preincubated with or without 1 μM Fer-1 (HY-100579, MedChemExpress) for 1 h. Subsequently, 10 or 20 μM OP-B was added to AGS and NCI-N87 cells and incubated for another 24 h at 37˚C. Subsequently, the cells were stained with 1 ml of 1 μM 2',7'-dichlorofluorescein diacetate (DCFDA) probe for 30 min at room temperature. The cells were washed with PBS three times (5 min/wash) and observed under a fluorescence microscope (x20, Olympus, Japan).

In vivo assay. Four- to six-week-old female nude mice were purchased from the Peking University Health Science Center (Beijing, China). AGS cells ($1x10^6$ cells, total volume: 100 μl in

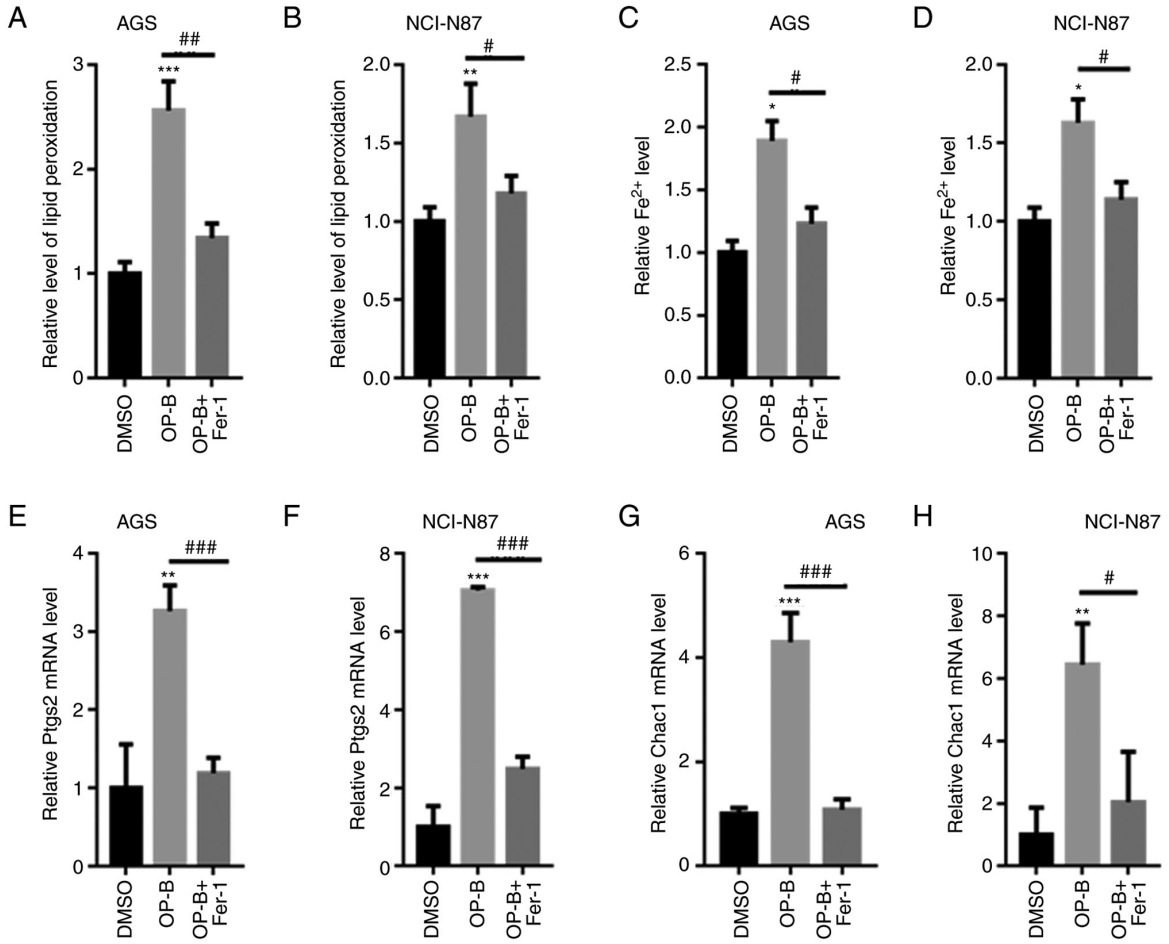

Figure 4. OP-B increased the production of MDA and Fe^{2+} in AGS and NCI-N87 cells. OP-B significantly increased the MDA content, but preincubation with Fer-1 decreased the OP-B-induced increase in the MDA content in (A) AGS and (B) NCI-N87 cells. OP-B also increased Fe^{2+} levels in (C) AGS and (D) NCI-N87 cells. OP-B treatment increased the Ptgs2 and Chac1 mRNA levels, but preincubation with Fer-1 reversed these effects on (E and G) AGS and (F and H) NCI-N87 cells. *P<0.05, **P<0.01, and ***P<0.001 compared with DMSO; $^{\#}$P<0.05, $^{\#\#}$P<0.01, $^{\#\#\#}$P<0.001 vs. OP-B group.

PBS) were injected into the right posterior flanks of the nude mice [5 mice/group (n=70 total animals), weight: 14-16 g]. Animal handling and research protocols were approved by the Ethics Committee of Jiaozhou Central Hospital (JCH-209ZH35). All mice were housed in a temperature-(20-24˚C) and humidity-controlled (45-55%) environment with free access to food and water. A 12/12h light/dark cycle was maintained in the animal housing rooms. Seven days later, tumor-bearing mice were randomly divided into two groups, including those treated with OP-B (100 μl, 50 mg/kg p.o. daily; n=5) or CMC-Na (control, 100 μl, p.o. daily; n=5) for 14 days. To evaluate tumor growth, 5 mice/group were sacrificed every two days prior to sacrifice on day 14. Finally, after 14 days, the mice were euthanized by administering an intraperitoneal injection of pentobarbital sodium (110 mg/kg) (21), and the tumors were collected for further analysis. Tumor volumes were calculated using the formula: volume=(length x width^2)/2.

Statistical analysis. SPSS 13.0; SPSS, Inc. was used to analyze the data. The data are presented as the means ± standard deviations from three independent experiments. A Wilcoxon signed-rank test was performed to compare ptgs2 and chac1 mRNA levels between GC tissues and adjacent normal control tissues. Unpaired Student's t-tests were used for comparisons between two groups. Analysis of variance followed by Tukey's post hoc test were used for comparisons of more than 2 groups. P<0.05 was considered to indicate a statistically significant difference.

Results

Decreased levels of the Ptgs2 and Chac1 mRNAs in GC tissues. First, the mRNA levels of ferroptosis markers, including prostaglandin-endoperoxide synthase 2 (Ptgs2) and ChaC glutathione-specific gamma-glutamylcyclotransferase 1 (Chac1) were determined. qPCR analysis revealed significantly reduced levels of the Ptgs2 and Chac1 mRNAs in GC tissues compared with those in adjacent normal control tissues (Fig. 1A and B), indicating that ferroptosis was suppressed in GC tissues.

OP-B reduced AGS and NCI-N87 cell viability in a dose- and time-dependent manner. GC cells were treated with different concentrations of OP-B as aforementioned. As shown in Fig. 2A and B, treatment with OP-B decreased the viability of AGS and NCI-N87 cells in a dose-dependent manner. The IC_{50} for AGS cells was 10.27 μM and for NCI-N87 cells it was 21.32 μM. Subsequently, AGS and NCI-N87 cells with 10 or

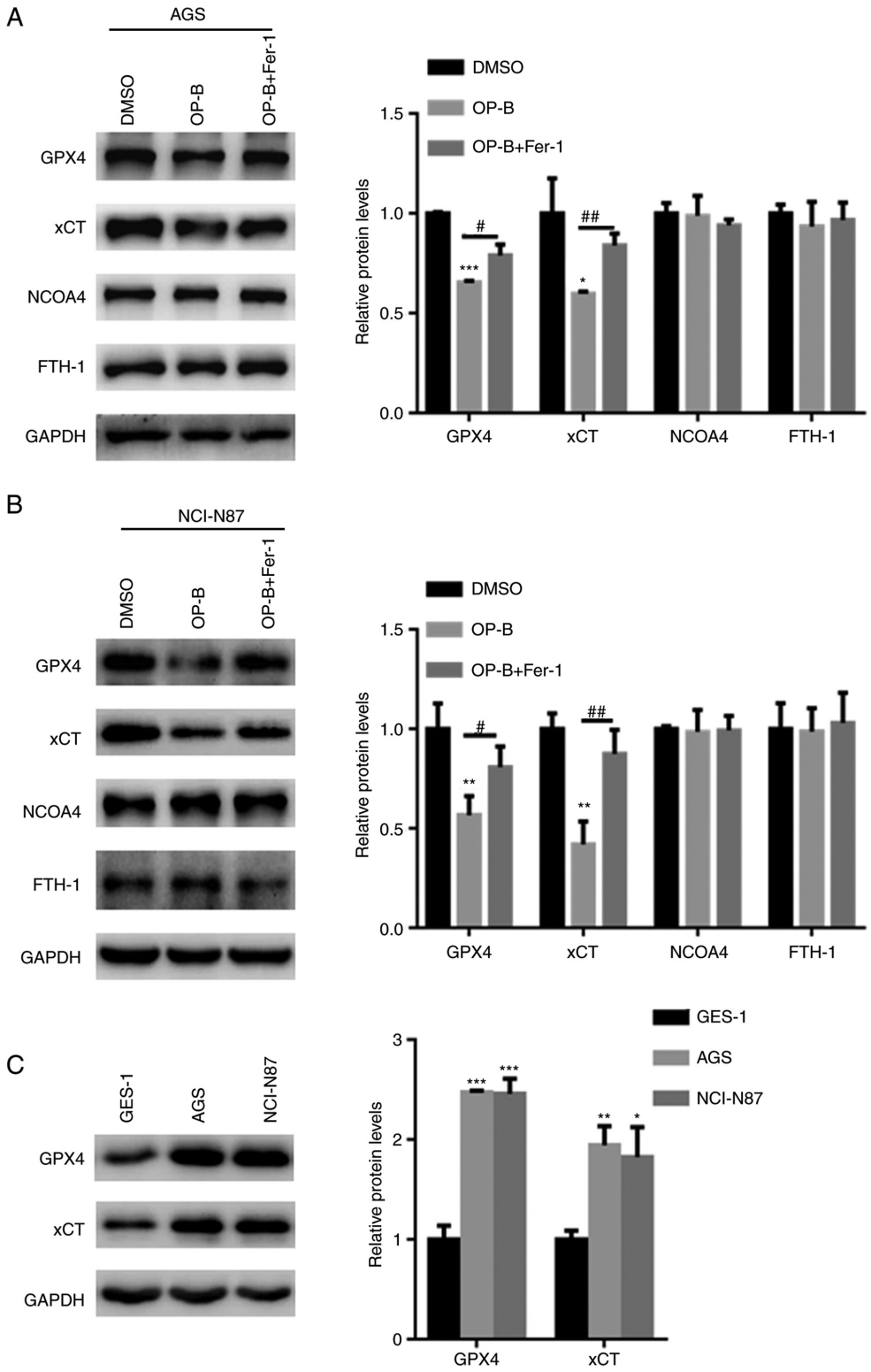

Figure 5. OP-B reduced the expression of GPX4 and xCT in GC cells. Western blot analysis revealed that OP-B reduced the expression of GPX4 and xCT in both (A) AGS and (B) NCI-N87 cells, but no changes in the expression of NCOA4 and FTH-1 was detected. (C) Compared with that in GES-1 cells, the expression of GPX4 and xCT was upregulated in those of AGS and NCI-N87 cells. *P<0.05, **P<0.01, and ***P<0.001 compared with DMSO; $^{\#}$P<0.05, $^{\#\#}$P<0.01 vs. OP-B group.

20 μM OP-B, respectively. OP-B decreased the viability of AGS and NCI-N87 cells at 12, 24, 48 and 72 h (Fig. 2C and D).

OP-B induced ferroptosis in AGS and NCI-N87 cells. AGS and NCI-N87 cells were treated with 10 or 20 μM OP-B to explore whether OP-B induces ferroptosis in GC cells. As shown in Fig. 3A and B, preincubation with a pancaspase inhibitor (benzyloxycarbonyl-Val-Ala-Asp-fluoromethyl ketone, zVAD-fmk), necrosis inhibitor (necrostatin-1, Nec-1), or autophagy inhibitor (3-methyladenine, 3-MA) did not

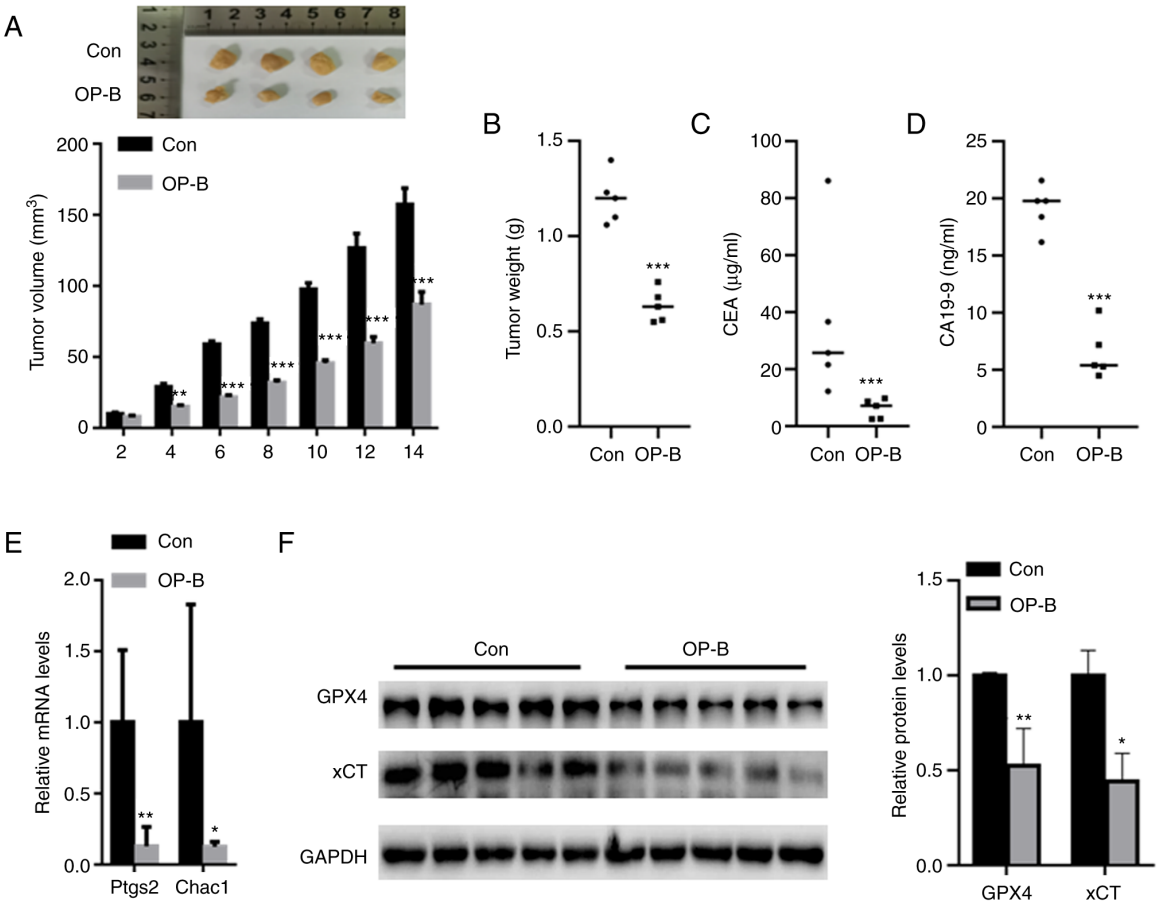

Figure 6. OP-B suppressed tumor growth *in vivo*. (A) The mice (5 mice/group) in the control and OP-B groups were sacrificed at day 2, 4, 6, 8, 10, 12 and 14, respectively. OP-B treatment significantly decreased xenograft tumor growth compared with that of the control. When the mice (5 mice/group) grew until 14 days, the tumor weight, CEA level, CA19-9 level, Ptgs2 and Chac1 mRNA level, as well as the corresponding protein expression were determined. (B) Compared with the control group, the tumor weight was also significantly decreased in the OP-B group. Serum levels of GC biomarkers, including (C) CEA and (D) CA19-9, were also decreased in the OP-B group compared with the control group. (E) qPCR analysis indicated that OP-B significantly reduced the mRNA levels of Ptgs2 and Chac1 compared with those of the control group. (F) Western blot analysis revealed significantly decreased GPX4 and xCT levels in the tumor tissues from the OP-B group compared to those from the control group. *P<0.05, **P<0.01, and ***P<0.001 compared with the indicated groups.

abolish OP-B-induced GC cell death. However, pretreatment with the ferropotosis inhibitor Fer-1 significantly reversed AGS and NCI-N87 cell death induced by OP-B (Fig. 3A and B). DCFDA staining showed that OP-B increased the ROS contents in AGS and NCI-NC87 cells, but a preincubation with Fer-1 reversed the increased production of ROS induced by OP-B (Fig. 3C and D). The flow cytometric analysis indicated that OP-B significantly induced AGS and NCI-N87 cell death, while a preincubation with Fer-1 partially reversed OP-B-induced GC cell death (Fig. 3E and F).

OP-B increased the production of MDA and Fe^{2+}. MDA and ROS contents were quantified in AGS and NCI-N87 cells. As shown in Fig. 4A and B, OP-B significantly increased the MDA content, but preincubation with Fer-1 decreased the higher MDA content induced by OP-B in both AGS and NCI-N87 cells. OP-B also increased Fe^{2+} levels in AGS and NCI-N87 cells (Fig. 4C and D). In addition, the levels of ferroptosis-related markers, including Ptgs2 and Chac1, were significantly increased by OP-B treatment, but preincubation with Fer-1 reversed these effects (Fig. 4E-H). These data further validated that OP-B induced GC cell ferroptosis.

OP-B reduced GPX4 and xCT expression in GC cells. The underlying mechanism by which OP-B induced ferroptosis in GC cells was examined. Western blot analysis revealed that OP-B reduced the expression of GPX4 and xCT in both AGS and NCI-N87 cells (Fig. 5A and B). By contrast, pretreatment with Fer-1 partially reversed the OP-B-induced reductions in GPX4 and xCT levels in AGS and NCI-N87 cells (Fig. 5A and B). However, OP-B did not alter the expression of NCOA4 and FTH-1, two important ferritinophagy markers (Fig. 5A and B). Furthermore, the expression of GPX4 and xCT gene was explored in gastric cancer and normal cells. Compared with that in GES-1 cells, the expression of GPX4 and xCT was upregulated in those of AGS and NCI-N87 cells (Fig. 5C).

OP-B suppressed tumor growth in vivo. In vivo assays showed that OP-B treatment significantly decreased xenograft tumor growth after six days compared with that of the control (Fig. 6A). After 14 days, the final tumor volumes in the OP-B and control groups were 85.7±8.5 mm^3 and 158.35±12.3 mm^3, respectively. Compared with the control group, the tumor weight was also significantly decreased in the OP-B group (Fig. 6B). In addition, the levels of GC biomarkers, including CEA and CA19-9, were also decreased in the serum of the OP-B group compared with

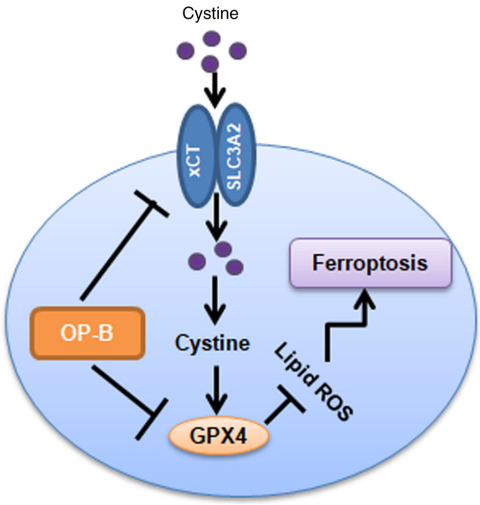

Figure 7. A diagram indicating how ferroptosis pathways are promoted by OP-B.

the control group (Fig. 6C and D). qPCR analysis indicated that OP-B significantly reduced the mRNA levels of Ptgs2 and Chac1 compared with those of the control group (Fig. 6E). Western blot analysis revealed a significantly decreased expression of GPX4 and xCT in the tumor tissues from the OP-B group compared to those from the control group (Fig. 6F).

Discussion

Ferroptosis is a novel characterized form of regulated cell death that is induced by excess intracellular ROS and iron levels (9). Nanotargeting of withaferin efficiently leads to ferroptosis and exerts satisfactory effects on neuroblastoma (22). In addition, anticancer drugs, including lapatinib and siramesine, have been shown to induce ferroptosis (23). Based on these findings, ferroptosis is involved in the anticancer effects of drugs. However, researchers have not clearly determined whether OP-B induces ferroptosis in GC cells.

Recent studies have confirmed that ferroptosis plays a key role in the evolution of GC (15-17). Consistent with these findings, data of the present study showed significantly increased levels of ferroptosis biomarkers, including Ptgs2 and Chac1, in GC tissues compared with adjacent normal control tissues. The CCK-8 assay indicated that OP-B reduced GC cell viability in a time- and dose-dependent manner. These findings indicated a tumor suppressor function of OP-B in GC cells.

OP-B was administered in combination with different cell death inhibitors, including zVAD, Nec-1, 3-MA and Fer-1. The results of the present study showed that only the ferroptosis inhibitor Fer-1 abolished the OP-B-induced death of both AGS and NCI-N87 cells, but not the other inhibitors. Furthermore, OP-B significantly increased the production of ROS, MDA and Fe^{2+}, but preincubation with Fer-1 abolished these effects. Flow cytometry also confirmed that OP-B increased AGS and NCI-NC87 cell death. These findings suggest that, OP-B may induce GC cell ferroptosis, thereby inhibiting GC.

One of the roles of GPX4 is to block lipid ROS production, and suppression of GPX4 results in the accumulation of lipid ROS, thereby inducing ferroptosis in various cells (24,25). xCT is composed of cystine/glutamate transporters, and it mainly provides a substrate for glutathione synthesis (10). The inhibition of xCT would decrease the capacity of GPX4 to clear lipid ROS via inadequate glutathione synthesis and finally induce cell death (10,26). According to results of the present study, OP-B suppressed the expression of GPX4 and xCT, suggesting that OP-B-induced ferroptotic cell death may be achieved by inhibiting the GPX4/xCT system.

Considering the effect dose and toxicity dose of OP-B in *in vivo* studies, it has been reported that 75 mg/kg OP-B significantly decreases the number of A-549-related metastatic nodules in contrast to the control treatment group (27). In addition, the toxicity effects of OP-B were evaluated in ovarian cancer cells in nude mice *in vivo* (28). The results show that both 15 and 75 mg/kg OP-B do not lead to cell degeneration, necrosis, or infiltration of inflammatory factors in heart, liver, lung, and kidney *in vivo* (28). Thus, 50 mg/kg OP-B was selected in the present study while 50 mg/kg OP-B did not demonstrate toxicity. The *in vivo* results were consistent with the *in vitro* experiments. *In vivo* administration of OP-B reduced the volume and weight of AGS tumors. In addition, expression of GPX4 and xCT was suppressed in nude mice treated with OP-B compared with control mice.

However, there are limitations to the present study. First, we did not explore the expression of each gene in the 60 GC and adjacent normal control specimens. In future studies, analysis via western blot and RT-qPCR. Secondly, results of the present study showed that OP-B had an IC_{50} of 10-20 μM. Investigation as to whether these results are comparable to clinical plasma concentration in patients should be conducted. Thirdly, novel data that OP-B induced GC cell death via GPX4 and xCT were identified; however, whether GPX4 or xCT contributes more to the OP-B-induced ferroptosis deserves further study. Fourthly, a future aim is the translation of the current results into a clinical trial, which may ameliorate the employment of OP-B in clinic.

In summary, OP-B induces ferroptosis in gastric cancer cells by inhibiting the transplasma membrane cysteine redox shuttle mediated by blocking the GPX4/xCT system (Fig. 7).

Acknowledgements

Not applicable.

Funding

The present study was supported by a grant from the Hunan Province Supporting Fund of Jiaozhou Central Hospital (HNJ-20B76CD).

Availability of data and materials

The datasets used and/or analyzed during the current study are available from the corresponding author upon reasonable request.

Authors' contributions

LZ performed the experiments, analyzed the data and wrote the manuscript. CL, YZ, and JZ performed the RT-qPCR experiments. XY designed the experiments, analyzed the data

and provided final approval of the version to be published. LZ and XY confirm the authenticity of all the raw data. All authors read and approved the final manuscript.

Ethics approval and consent to participate

The present study was approved by the Ethics Committee of Jiaozhou Central Hospital. Animal handling and research protocols were approved by the Ethics Committee of Jiaozhou Central Hospital (JCH-209ZH35). The approval human protocol number was JCH-209ZH36, and all the participants provided written informed consent.

Patient consent for publication

Not applicable.

Competing interests

The authors have no competing interests to declare.

References

1. Ma H, Lian C and Song Y: Fibulin-2 inhibits development of gastric cancer by downregulating β-catenin. Oncol Lett 18: 2799-2804, 2019.
2. Niu J, Song X and Zhang X: Regulation of lncRNA PVT1 on miR-125 in metastasis of gastric cancer cells. Oncol Lett 19: 1261-1266, 2020.
3. Sun Y, Zhao C, Ye Y, Wang Z, He Y, Li Y and Mao H: High expression of fibronectin 1 indicates poor prognosis in gastric cancer. Oncol Lett 19: 93-102, 2020.
4. Bersuker K, Hendricks JM, Li Z, Magtanong L, Ford B, Tang PH, Roberts MA, Tong B, Maimone TJ, Zoncu R, *et al*: The CoQ oxidoreductase FSP1 acts parallel to GPX4 to inhibit ferroptosis. Nature 575: 688-692, 2019.
5. Gong Y, Wang N, Liu N and Dong H: Lipid peroxidation and GPX4 inhibition are common causes for myofibroblast differentiation and ferroptosis. DNA Cell Biol 38: 725-733, 2019.
6. Ingold I, Berndt C, Schmitt S, Doll S, Poschmann G, Buday K, Roveri A, Peng X, Freitas FP, Seibt T, *et al*: Selenium utilization by GPX4 is required to prevent hydroperoxide-induced ferroptosis. Cell 172: 409-422 e421, 2018.
7. Ni J, Chen K, Zhang J and Zhang X: Inhibition of GPX4 or mTOR overcomes resistance to lapatinib via promoting ferroptosis in NSCLC cells. Biochem Biophys Res Commun 567: 154-160, 2021.
8. Seibt TM, Proneth B and Conrad M: Role of GPX4 in ferroptosis and its pharmacological implication. Free Radic Biol Med 133: 144-152, 2019.
9. Song X, Wang X, Liu Z and Yu Z: Role of GPX4-mediated ferroptosis in the sensitivity of triple negative breast cancer cells to gefitinib. Front Oncol 10: 597434, 2020.
10. Lee N, Carlisle AE, Peppers A, Park SJ, Doshi MB, Spears ME and Kim D: xCT-Driven expression of GPX4 determines sensitivity of breast cancer cells to ferroptosis inducers. Antioxidants (Basel) 10: 317, 2021.
11. Koppula P, Zhuang L and Gan B: Cystine transporter SLC7A11/xCT in cancer: Ferroptosis, nutrient dependency, and cancer therapy. Protein Cell 12: 599-620, 2021.
12. Zhang Y, Kong Y, Ma Y, Ni S, Wikerholmen T, Xi K, Zhao F, Zhao Z, Wang J, Huang B, *et al*: Loss of COPZ1 induces NCOA4 mediated autophagy and ferroptosis in glioblastoma cell lines. Oncogene 40: 1425-1439, 2021.
13. Fang Y, Chen X, Tan Q, Zhou H, Xu J and Gu Q: Inhibiting ferroptosis through disrupting the NCOA4-FTH1 interaction: A new mechanism of action. ACS Cent Sci 7: 980-989, 2021.
14. Tsai Y, Xia C and Sun Z: The inhibitory effect of 6-gingerol on ubiquitin-specific peptidase 14 enhances autophagy-dependent ferroptosis and anti-tumor in vivo and in vitro. Front Pharmacol 11: 598555, 2020.
15. Ma R, Shimura T, Yin C, Okugawa Y, Kitajima T, Koike Y, Okita Y, Ohi M, Uchida K, Goel A, *et al*: Antitumor effects of andrographis via ferroptosis-associated genes in gastric cancer. Oncol Lett 22: 523, 2021.
16. Zhao L, Peng Y, He S, Li R, Wang Z, Huang J, Lei X, Li G and Ma Q: Apatinib induced ferroptosis by lipid peroxidation in gastric cancer. Gastric Cancer 24: 642-654, 2021.
17. Guan Z, Chen J, Li X and Dong N: Tanshinone IIA induces ferroptosis in gastric cancer cells through p53-mediated SLC7A11 down-regulation. Biosci Rep 40: BSR20201807, 2020.
18. Gao GY, Ma J, Lu P, Jiang X and Chang C: Ophiopogonin B induces the autophagy and apoptosis of colon cancer cells by activating JNK/c-Jun signaling pathway. Biomed Pharmacother 108: 1208-1215, 2018.
19. Chen M, Guo Y, Zhao R, Wang X, Jiang M, Fu H and Zhang X: Ophiopogonin B induces apoptosis, mitotic catastrophe and autophagy in A549 cells. Int J Oncol 49: 316-324, 2016.
20. Zhang W, Zhang Q, Jiang Y, Li F and Xin H: Effects of ophiopogonin B on the proliferation and apoptosis of SGC7901 human gastric cancer cells. Mol Med Rep 13: 4981-4986, 2016.
21. Aartsen WM, Schuijt MP, Danser AH, Daemen MJAP and Smits JFM: The role of locally expressed angiotensin converting enzyme in cardiac remodeling after myocardial infarction in mice. Cardiovasc Res 56: 205-213, 2002.
22. Hassannia B, Wiernicki B, Ingold I, Qu F, Van Herck S, Tyurina YY, Bayır H, Abhari BA, Angeli JPF, Choi SM, *et al*: Nano-targeted induction of dual ferroptotic mechanisms eradicates high-risk neuroblastoma. J Clin Invest 128: 3341-3355, 2018.
23. Ma S, Henson ES, Chen Y and Gibson SB: Ferroptosis is induced following siramesine and lapatinib treatment of breast cancer cells. Cell Death Dis 7: e2307, 2016.
24. Vuckovic AM, Bosello Travain V, Bordin L, Cozza G, Miotto G, Rossetto M, Toppo S, Venerando R, Zaccarin M, Maiorino M, *et al*: Inactivation of the glutathione peroxidase GPx4 by the ferroptosis-inducing molecule RSL3 requires the adaptor protein 14-3-3ε. FEBS Lett 594: 611-624, 2020.
25. Wang S, Liu W, Wang J and Bai X: Curculigoside inhibits ferroptosis in ulcerative colitis through the induction of GPX4. Life Sci 259: 118356, 2020.
26. Wang H, Peng S, Cai J and Bao S: Silencing of PTPN18 induced ferroptosis in endometrial cancer cells through p-P38-mediated GPX4/xCT down-regulation. Cancer Manag Res 13: 1757-1765, 2021.
27. Chen M, Hu C, Guo Y, Jiang R, Jiang H, Zhou Y, Fu H, Wu M and Zhang X: Ophiopogonin B suppresses the metastasis and angiogenesis of A549 cells *in vitro* and *in vivo* by inhibiting the EphA2/Akt signaling pathway. Oncol Rep 40: 1339-1347, 2018.
28. Yuan S, Xu Y, Yi T and Wang H: The anti-tumor effect of OP-B on ovarian cancer in vitro and in vivo, and its mechanism: An investigation using network pharmacology-based analysis. J Ethnopharmacol 283: 114706, 2021.